

Δ_T Noise from Electron–Hole Asymmetry in Normal and Superconducting Quantum Point Contacts

Sachiraj Mishra^{1,2,*} and Colin Benjamin^{1,2,†}

¹*School of Physical Sciences, National Institute of Science Education and Research, HBNI, Jatni-752050, India*

²*Homi Bhabha National Institute, Training School Complex, AnushaktiNagar, Mumbai, 400094, India*

This work examines Δ_T noise in two-terminal hybrid nanostructures featuring a quantum point contact (QPC), realized either between two normal metals (NQN) or between a normal metal and a superconductor (NQS). The inclusion of a QPC breaks electron-hole (e-h) symmetry, leading to a finite thermovoltage. In contrast, earlier studies on hybrid junctions incorporating insulating barriers, as e-h symmetry is preserved, have vanishing thermovoltage, and consequently, Δ_T noise is calculated at zero thermovoltage. In our setup, the broken e-h symmetry allows for a finite thermovoltage, at which we compute the corresponding Δ_T noise. Unlike earlier studies restricted by e-h symmetry and vanishing thermovoltage, our work establishes a self-consistent framework in mesoscopic hybrid junctions, revealing how Andreev reflection fundamentally reshapes Δ_T noise once e-h symmetry is broken. This broad access to charge fluctuation signatures provides a more comprehensive understanding of non-equilibrium transport in linear response. To our knowledge, this work provides the first self-consistent analysis of Δ_T noise in superconducting hybrid junctions where e-h symmetry is broken, explicitly revealing how Andreev reflection modifies Δ_T noise beyond the symmetry-protected zero-thermovoltage regime.

I. Introduction

The study of Δ_T noise has recently attracted considerable attention from both theoretical and experimental [1–18] perspectives. Experimental realizations have demonstrated the presence of Δ_T noise across a broad range of mesoscopic platforms, including single-molecule transport setups [10], engineered quantum electronic circuits [11], and metallic tunnel structures subjected to thermal gradients [12]. Δ_T noise refers to the quantum shot noise-like component that remains finite when a temperature difference is applied across the system while the net charge current vanishes [1, 4, 10]. As such, it serves as a powerful probe of nonequilibrium quantum transport processes driven purely by thermal bias.

We investigate charge Δ_T noise in normal metal–quantum point contact–normal metal (NQN) and normal metal–quantum point contact–superconductor (NQS) junctions, and present a comparative analysis with the corresponding charge quantum shot noise under finite charge current. In our earlier work [13], we studied charge Δ_T noise, defined at vanishing charge current, in electron-hole (e-h) symmetric systems such as normal metal-insulator-normal metal (NIN) and normal metal-insulator-superconductor (NIS) junctions. In these symmetric setups, the charge thermovoltage vanishes when charge current vanishes, so the Δ_T noise is evaluated strictly at this condition. In contrast, the NQN and NQS junctions explicitly break e-h symmetry, allowing a finite thermovoltage to develop under a thermal bias to maintain zero net charge current. This asymmetry enables us to investigate how a finite thermovoltage influences the charge Δ_T noise. The breaking of e-h symmetry in NQN and NQS junctions thus provides a unique platform to explore charge Δ_T noise, offering new insights into nonequilibrium transport phenomena in mesoscopic hybrid systems, insights that are inaccessible in e-h symmetric NIN and NIS junctions.

In this work, we uncover several key distinctions in the noise characteristics of quantum point contact (QPC)-based NQN and NQS junctions, in contrast to their insulating counterparts, namely, NIN and NIS junctions. When analyzing the charge Δ_T noise in NQN and NQS systems, we observe pronounced oscillations as a function of Fermi energy, features that are absent in the NIN and NIS cases, as reported in Ref. [13]. A similar oscillatory pattern is also observed in quantum shot noise evaluated at finite charge current. Notably, the enhancement observed for Δ_T noise when comparing the NQS junction with its NQN counterpart is bounded by a maximum value of 16, consistent with earlier findings for NIS and NIN junctions in the regime of transparent limit [13]. However, the ratio reduces from 16 as temperature increases. This reduction arises from increased thermal excitations at higher temperatures, which promote quasiparticle transport above the superconducting gap. A similar temperature-induced suppression is also observed in the NIN and NIS setups, see [13].

The remainder of this article is organized as follows: In Sec. II, we outline the theoretical framework underlying our analysis. We begin with a brief overview of the Landauer–Büttiker formalism for mesoscopic systems and then describe quantum transport in both NQN and NQS junctions. This section also presents the general theory of quantum charge noise, followed by the formulation for calculating charge thermovoltages and charge Δ_T noise in the NQN and NQS setups at finite thermovoltage. Section III presents our main results on charge Δ_T noise, along with the corresponding quantum shot noise evaluated under finite charge current induced by a voltage bias. In Sec. IV, we carry out a detailed comparison of the charge Δ_T noise as well as normalized Δ_T noise both in the NQN and NQS junctions, including the evaluation of their respective ratios. Finally, Sec. V summarizes the key findings of our study and discusses prospects for experimental realization. Detailed derivations of scattering amplitudes in the NQS junction, expressions for charge current, thermovoltage, and quantum and Δ_T noise formulations are provided in Appendices A–C. The MATHEMATICA code used to compute the conductance, thermovoltage, quantum shot noise, and Δ_T noise

* sachiraj29mishra@gmail.com

† colin.nano@gmail.com

is provided in Ref. [19].

II. Theory

The Landauer-Büttiker formalism is a powerful tool for studying transport in systems exhibiting ballistic conduction. According to this approach, charge current is directly proportional to the net transmission probability of electron scattering between terminals. This formalism has proven invaluable for analyzing various junctions, including QPCs [20–25] in normal metals, NIN and NIS junctions. In the following sections, we delve into the details of these configurations to understand the transport properties and underlying physical mechanisms.

A. Landauer-Büttiker Formalism

In the next two subsections, we specifically discuss the charge current formula in two terminal junctions, first normal metal-QPC-normal metal junction (NQN) and then normal metal-QPC-superconductor (NQS) junction.

1. NQN Junction

Using the Landauer-Büttiker approach, the average charge current at terminal α ($\langle I_\alpha \rangle$) in a multiterminal normal-state conductor is written as [20, 26]:

$$\langle I_\alpha \rangle = \frac{2q}{h} \sum_\beta \int_{-\infty}^{\infty} dE' (\delta_{\alpha\beta} - T_{\alpha\beta}) [f_\alpha(E') - f_\beta(E')], \quad (1)$$

where $T_{\alpha\beta}(E')$ is the energy-dependent transmission probability from terminal β to α , where E' is the total energy and $f_\alpha(E')$ is the Fermi-Dirac distribution in terminal α , given by

$$f_\alpha = \frac{1}{1 + e^{(E' - \mu_\alpha)/k_B T_\alpha}}. \quad (2)$$

Here, $\mu_\alpha = E_F + qV_\alpha$ is the chemical potential in terminal α . E_F denotes the Fermi level, V_α represents the applied voltage bias in terminal α , and $T_\alpha = T + \Delta T_\alpha$ is the temperature of terminal α , with T taken as the reference temperature of the system and ΔT_α describing the imposed thermal offset at terminal α . The quantity q specifies the quasiparticle charge, taking the value $q = e$ for electron-like excitations and $q = -e$ for hole-like excitations.

In the linear response regime, i.e., when $qV_\alpha \ll E_F$ and $\Delta T_\alpha \ll T$, the charge current can be expressed as [20, 26]:

$$\langle I_\alpha \rangle = \sum_\beta G_{\alpha\beta} V_\beta + \Pi_{\alpha\beta} \Delta T_\beta. \quad (3)$$

The transport coefficients in this expression are defined as:

Charge conductance: $G_{\alpha\beta}$

$$= \frac{2q^2}{h} \int_{-\infty}^{\infty} dE (\delta_{\alpha\beta} - T_{\alpha\beta}) (-\partial f / \partial E),$$

Seebeck coefficient: $S_{\alpha\beta} = \frac{\Pi_{\alpha\beta}}{G_{\alpha\beta}}$ with,

$$\Pi_{\alpha\beta} = \frac{2q}{hT} \int_{-\infty}^{\infty} dE (\delta_{\alpha\beta} - T_{\alpha\beta}) (E) (-\partial f / \partial E), \quad (4)$$

where, E being the excitation energy, i.e., $E = E' - E_F$, $f = (1 + e^{E/k_B T})^{-1}$ is the equilibrium Fermi-Dirac distribution and h being the Planck's constant.

In NQN junction, see Fig. 1, in contrast to the NIN junction, where electron-hole symmetry ensures that the transmission probability is an even function of energy, explicitly breaks this symmetry, as the transmission probability via a QPC is asymmetric with respect to energy. As a result, in a NIN junctions, the off-diagonal Onsager coefficients such as $\Pi_{\alpha\beta}$ vanishes, leading to zero charge current under zero applied voltage bias [13]. However, in a NQN configuration, $\Pi_{\alpha\beta}$ is finite, allowing for finite charge thermovoltages in the absence of net charge current.

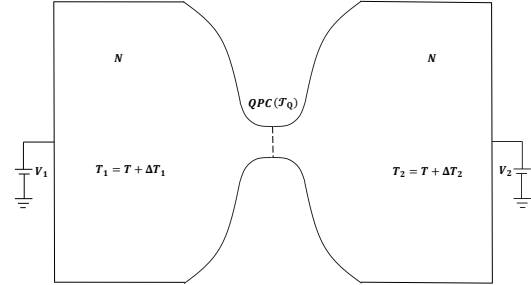


Figure 1: Schematic diagram of the NQN junction. The black dashed line in the middle represents the QPC constriction. We consider $V_1 = \Delta V$, $V_2 = 0$, $\Delta T_1 = -\Delta T_2 = \Delta T/2$.

The quantum point contact (QPC) was originally introduced in Ref. [27] to study conductance quantization in the ballistic transport regime. Since then, it has been widely used in the study of thermoelectric effects [21–24]. The potential landscape of the QPC is modeled by the following confinement potential [27]:

$$U(x, y) = \frac{1}{2} m^* \omega_y^2 y^2 - \frac{1}{2} m^* \omega_x^2 x^2 + V_0, \quad (5)$$

where m^* being the electron's effective mass, and V_0 is the potential offset. The energy levels in the QPC are quantized as $E_n = V_0 + (n + 1/2)\hbar\omega_y$. The corresponding transmission probability for the n th mode as derived in Ref. [27] is given as,

$$T_Q(E) = \left(1 + e^{-2\pi(E + E_F - E_n)/\hbar\omega_x} \right)^{-1}. \quad (6)$$

To compute the charge current in the NQN junction as shown in Fig. 1, we consider voltage bias applied in the left normal metal as $V_1 = \Delta V$ and in the right normal metal as $V_2 = 0$. The left normal-metal lead is maintained at a temperature $T_1 = T + \Delta T_1$, while the right normal-metal lead is held at $T_2 = T + \Delta T_2$, where $\Delta T_1 = -\Delta T_2 = \Delta T/2$, see Fig. 1. An electron incident from the left normal-metal lead is reflected back with probability $1 - \mathcal{T}_Q$, while its transmission across the QPC into the right lead occurs with probability \mathcal{T}_Q . Thus, according to Eq. (3), the charge current in terminal 1 are given by

$$\langle I_1^{NQN} \rangle = G_{NQN} \Delta V + \Pi_{NQN} \Delta T, \quad (7)$$

where,

$$\begin{aligned} G_{NQN} &= \frac{2e^2}{h} \int_{-\infty}^{\infty} dE \mathcal{T}_Q(E) (-\partial f / \partial E), \\ \Pi_{NQN} &= \frac{2e}{hT} \int_{-\infty}^{\infty} dE \mathcal{T}_Q(E) \cdot (-\partial f / \partial E). \end{aligned} \quad (8)$$

Here, the charge current $\langle I_1^{NQN} \rangle$ vanishes at a finite charge thermovoltage, given by $V_{th}^{NQN} = \frac{-\Pi_{NQN}}{G_{NQN}} \Delta T = -S_{NQN} \Delta T$. S_{NQN} is the Seebeck coefficient in the NQN junction. For multichannel transport ($n > 1$), the zero-temperature charge conductance becomes $G_{NQN} = \frac{2e^2}{h} \sum_n \mathcal{T}_Q$. We now turn to the NQS junction and discuss the general formula for charge current as well as charge thermovoltage.

2. NQS Junction

Similarly, in a multiterminal normal metal-superconductor junction, the charge current out of a normal metallic terminal is given as [20],

$$\langle I_\alpha \rangle = \frac{2e}{h} \sum_{\beta} \sum_{\rho, \xi \in \{e, h\}} \int_0^{\infty} dE \operatorname{sgn}(\rho) \left[\delta_{\alpha\beta} \delta_{\rho\xi} - \mathcal{T}_{\alpha\beta}^{\rho\xi} \right] f_{\beta}^{\xi}(E), \quad (9)$$

where, $f_{\beta}^{\xi}(E) = \frac{1}{1 + e^{\frac{E - \operatorname{sgn}(\xi) V_{th}}{k_B T_{\beta}}}}$, where $\operatorname{sgn}(\xi) = +1$ for electron and -1 for hole. Within the linear response framework, the charge current can be written in an analogous manner to Eq. (3), where the Onsager coefficients are [20],

Charge conductance:

$$G_{\alpha\beta} = \frac{2e^2}{h} \sum_{\rho, \xi \in \{e, h\}} \int_0^{\infty} dE \operatorname{sgn}(\rho) \operatorname{sgn}(\xi) (\delta_{\alpha\beta} \delta_{\rho\xi} - \mathcal{T}_{\alpha\beta}) \left(-\frac{\partial f}{\partial E} \right),$$

Seebeck coefficient: $S_{\alpha\beta} = \frac{\Pi_{\alpha\beta}}{G_{\alpha\beta}}$ with,

$$\Pi_{\alpha\beta} = \frac{2e}{hT} \sum_{\rho, \xi \in \{e, h\}} \int_0^{\infty} dE \operatorname{sgn}(\rho) (\delta_{\alpha\beta} \delta_{\rho\xi} - \mathcal{T}_{\alpha\beta}) (E) \left(-\frac{\partial f}{\partial E} \right). \quad (10)$$

We now consider a normal metal-quantum point contact-superconductor (NQS) junction, see Fig. 2. The relevant scattering amplitudes and probabilities are derived in Appendix A, following Refs. [28, 29].

The scattering processes in this hybrid junction include Andreev reflection probability: $\mathcal{R}^A(E)$, normal reflection probability: $\mathcal{R}^B(E)$, with the transmission probabilities $\mathcal{T}^C(E)$ and $\mathcal{T}^D(E)$ associated with electron-like and hole-like excitations, respectively. The net transmission probability across the NQS junction is given as [30] $\mathcal{T}_{NQS}(E) = 1 + \mathcal{R}^A(E) - \mathcal{R}^B(E)$ and it is derived in Appendix A and is given as

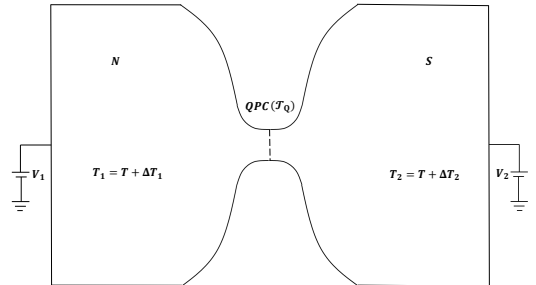


Figure 2: Schematic diagram of the NQS junction. The black dashed line in the middle represents the QPC constriction. We consider $V_1 = \Delta V$, $V_2 = 0$, $\Delta T_1 = -\Delta T_2 = \Delta T/2$.

$$\mathcal{T}_{NQS}(E) = \frac{\mathcal{T}_Q(E) - a^4 \mathcal{T}_Q(E) (1 - \mathcal{T}_Q(-E)) + \mathcal{T}_Q(E) \mathcal{T}_Q(-E) |a|^2}{(1 - \sqrt{1 - \mathcal{T}_Q(E)} \sqrt{1 - \mathcal{T}_Q(-E)} a^2)^2}, \quad (11)$$

where $a = \frac{v}{u}$ and $u(v) = \frac{1}{\sqrt{2}} \left(1 \pm \sqrt{\frac{E^2 - \Delta^2}{E^2}} \right)^{\frac{1}{2}}$ are the coherence factors in the superconductor, and $\Delta = 1.76 k_B T_C \sqrt{1 - \frac{T}{T_C}}$ with $T_C = 18K$ (for a s -wave superconductor like Nb_3Sn).

Now, similar to NQN junction, the average charge current $\langle I_1^{NQS} \rangle$ in the normal metal are expressed as

$$\langle I_1^{NQS} \rangle = G_{NQS} \Delta V + \Pi_{NQS} \Delta T, \quad (12)$$

where,

$$\begin{aligned}
G_{NQN} &= \frac{2e^2}{h} \int_{-\infty}^{\infty} dE (1 + \mathcal{R}^A(E) - \mathcal{R}^B(E)) (-\partial f / \partial E), \\
\Pi_{NQN} &= \frac{2e}{hT} \int_{-\infty}^{\infty} dE (1 + \mathcal{R}^A(E) - \mathcal{R}^B(E)).E.(-\partial f / \partial E).
\end{aligned} \tag{13}$$

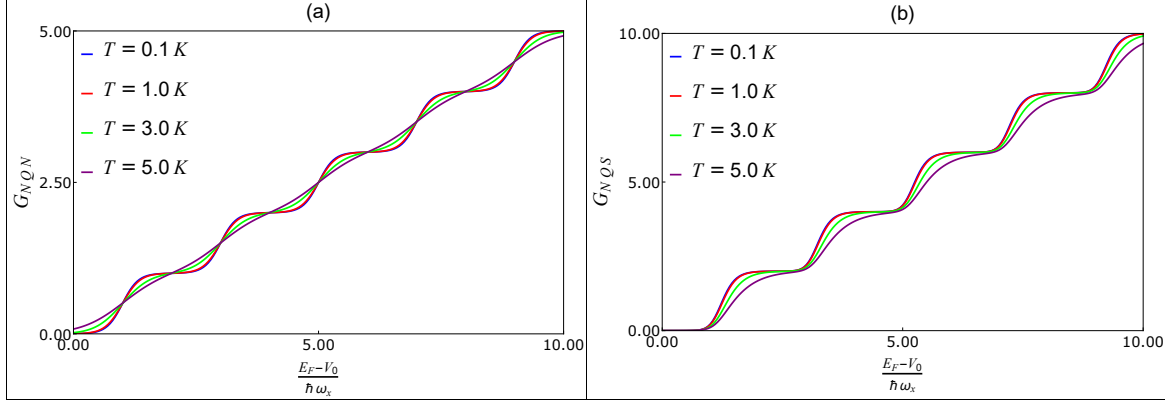


Figure 3: Charge conductance in (a) NQN (G_{NQN}) and (b) NQS (G_{NQS}) (in units of $\frac{2e^2}{h}$) vs. normalized Fermi energy ($\frac{E_F - V_0}{\hbar\omega_x}$) at different temperatures considered above. Parameters are taken are $\hbar\omega_y = 2.73\text{meV}$, $\hbar\omega_x = 0.5\hbar\omega_y$, where $T_C = 18\text{K}$.

In the NQN case, the charge current vanishes at a finite charge thermovoltage $V_{NQS}^{th} = \frac{-\Pi_{NQS}}{G_{NQS}} \Delta T = -S_{NQS} \Delta T$. S_{NQS} is the Seebach coefficient in the NQS junction. For multichannel transport ($n > 1$), the zero-temperature conductance below the superconducting energy gap Δ as shown in Refs. [28, 29] is given by $G_{NQS} = \frac{4e^2}{h} \sum_n \frac{T_Q^2}{(2 - T_Q)^2}$. This is also derived in Appendix A. In Fig. 3, we present the conductance profiles G_{NQN} and G_{NQS} as functions of the normalized Fermi energy $\frac{E_F - V_0}{\hbar\omega_x}$ for the transverse mode index $n = 4$, evaluated at various temperatures: $T = 1.0\text{K}, 3.0\text{K},$ and 5.0K . At $T = 1.0\text{K}$, both G_{NQN} and G_{NQS} exhibit well-defined quantized conductance plateaus as a function of $\frac{E_F - V_0}{\hbar\omega_x}$. As the temperature increases to $T = 3.0\text{K}$ and further to $T = 5.0\text{K}$, thermal broadening leads to a gradual smearing of these steps, and the conductance plateaus begin to diminish, eventually disappearing at higher temperatures. Notably, throughout the entire temperature range, the conductance G_{NQS} in the NQS junction remains consistently twice that of the G_{NQN} in the NQN junction. This doubling is attributed to Andreev reflection at the superconductor interface, where each incident electron is retroreflected as a hole, effectively contributing twice the charge to the conductance compared to the NQN case.

In the next section, we calculate the quantum noise as well as Δ_T noise in both NQN and NQS junctions.

B. Quantum Noise

Quantum noise, particularly the auto-correlation of charge current, plays a vital role in understanding fluctuation phenomena in mesoscopic systems. This section is focused on the charge quantum noise in NQN and NQS junctions, with particular emphasis on the zero-frequency limit.

1. NQN

This section presents an analysis of the charge quantum noise in the NQN junction, with the derivation provided in Appendix C. The total quantum noise is further decomposed into two distinct components: one is quantum thermal noise, and another is quantum shot noise.

The quantum noise autocorrelation characterizes fluctuations of the charge current flowing through the normal-metal lead of an NQN junction. More broadly, current-current correlations describing charge noise between terminals i and j , evaluated at times t and \bar{t} are defined as [25, 31] $Q_{ij}(t - \bar{t}) \equiv \langle \Delta I_i(t) \Delta I_j(\bar{t}) + \Delta I_j(\bar{t}) \Delta I_i(t) \rangle$, where $\Delta I_i(t) = I_i(t) - \langle I_i(t) \rangle$ denotes the current fluctuation at terminal i . Taking the Fourier transform yields the charge noise power spectrum: $\delta(\omega + \bar{\omega}) Q_{ij}(\omega) \equiv \frac{1}{2\pi} \langle \Delta I_i(\omega) \Delta I_j(\bar{\omega}) + \Delta I_j(\bar{\omega}) \Delta I_i(\omega) \rangle$, where ω and $\bar{\omega}$ are the frequencies associated with energy difference between incoming particles at two different times t and \bar{t} meaning if

E and \bar{E} are the energies of two different particles at time t , then $\omega = (E - \bar{E})/\hbar$ and at time \bar{t} , the difference in energy is

given by the frequency $\bar{\omega}$. The quantum noise correlation for the NQN junction for terminal $i = j = 1$ at vanishing frequency is given by [25, 31]:

$$\begin{aligned} Q_{11}^{NQN}(\omega = 0) &= \frac{2e^2}{h} \int \sum_{p,q \in \{1,2\}} A_{p;l}(1, E) A_{q;k}(1, E) [f_p(E)(1 - f_q(E)) + f_q(E)(1 - f_p(E))] dE \\ &= \frac{4e^2}{h} \left[\int_{-\infty}^{\infty} F_{11\text{th}}^{NQN} \sum_{i \in \{1,2\}} (f_{ie}(1 - f_{ie})) dE + \int_{-\infty}^{\infty} F_{11\text{sh}}^{NQN} (f_{1e} - f_{2e})^2 dE \right] = Q_{11\text{th}}^{NQN} + Q_{11\text{sh}}^{NQN}. \end{aligned} \quad (14)$$

Here, $A_{p;q}(1, E) = \delta_{1p}\delta_{1q} - s_{1p}^\dagger s_{1q}$ and $F_{11\text{th}}^{NQN} = \mathcal{T}_Q(E)$ and $F_{11\text{sh}}^{NQN} = \mathcal{T}_Q(E)(1 - \mathcal{T}_Q(E))$ are derived in Appendix C. The terms $Q_{11\text{th}}^{NQN}$ and $Q_{11\text{sh}}^{NQN}$ correspond to thermal and shot noise contributions, respectively.

2. NQS

In this section, we discuss quantum noise in NQS junction and also decompose it into two physical quantities called quan-

tum thermal noise and quantum shot noise.

Similarly for NQS junction, the current noise correlations between different quasiparticles (electrons and holes) has to be considered [31, 32]. The noise correlation function is defined as $Q_{ij}^{xy}(t - t') \equiv \langle \Delta I_i^x(t) \Delta I_j^y(t') + \Delta I_j^y(t') \Delta I_i^x(t) \rangle$, where $\Delta I_i^x(t) = I_i^x(t) - \langle I_i^x(t) \rangle$ and $x, y \in \{e, h\}$. Its frequency-domain representation is $\delta(\omega + \bar{\omega}) Q_{ij}^{xy}(\omega) \equiv \frac{1}{2\pi} \langle \Delta I_i^x(\omega) \Delta I_j^y(\bar{\omega}) + \Delta I_j^y(\bar{\omega}) \Delta I_i^x(\omega) \rangle$. The zero-frequency noise in an NQS junction is given by:

$$\begin{aligned} Q_{11}^{NQS}(\omega = 0) &= \frac{2e^2}{h} \int \sum_{\substack{p,q \in \{1,2\}, \\ \mu, v, \sigma, \rho \in \{e, h\}}} \text{sgn}(\mu) \text{sgn}(v) A_{p,\sigma;q,\rho}(1\mu) A_{q,\rho;p,\sigma}(1v) (f_{p\sigma}[1 - f_{q\rho}] + (1 - f_{p\sigma}) f_{q\rho}) dE, \\ &= Q_{11\text{th}}^{NQS} + Q_{11\text{sh}}^{NQS}, \end{aligned} \quad (15)$$

where $\text{sgn}(\mu) = +1$ for $x = e$ and -1 for $x = h$. Here, $A_{p,\sigma;q,\rho}(1\mu) = \delta_{1p}\delta_{1q}\delta_{\mu\sigma}\delta_{\mu\rho} - s_{1p}^{\mu\sigma*} s_{1q}^{\mu\rho}$ and V is the voltage bias

applied. The thermal and shot noise contributions, $Q_{11\text{th}}^{NQS}$ and $Q_{11\text{sh}}^{NQS}$, are derived in detail in Appendix C and they are given as,

$$\begin{aligned} Q_{11\text{th}}^{NQS} &= \frac{4e^2}{h} \int_{-\infty}^{\infty} dE \left[(1 - \mathcal{R}^B(E) + \mathcal{R}^A(E))^2 + \mathcal{R}^A(-E)\mathcal{R}^B(E) + \mathcal{R}^A(E)\mathcal{R}^B(-E) + \mathcal{R}^B(E)(\mathcal{T}^C(E) + \mathcal{T}^D(-E)) \right. \\ &\quad \left. + \mathcal{R}^A(E)(\mathcal{T}^D(E) + \mathcal{T}^C(-E) + 2\mathcal{R}^A(E)\mathcal{R}^B(E)) \right] f_{1e}(1 - f_{1e}) + \frac{4e^2}{h} \int_{-\infty}^{\infty} dE \left[\mathcal{T}^C(E)^2 + \mathcal{T}^D(E)^2 \right. \\ &\quad \left. + 2\mathcal{T}^C(E)\mathcal{T}^D(-E) + \mathcal{R}^B(E)(\mathcal{T}^C(E) + \mathcal{T}^D(-E)) + \mathcal{R}^A(E)(\mathcal{T}^C(-E) + \mathcal{T}^D(E)) \right] f_{2e}(1 - f_{2e}), \\ Q_{11\text{sh}}^{NQS} &= \frac{4e^2}{h} \int_{-\infty}^{\infty} dE \left[\mathcal{R}^B(E)(\mathcal{T}^C(E) + \mathcal{T}^D(-E)) + \mathcal{R}^A(E)(\mathcal{T}^C(-E) + \mathcal{T}^D(E)) + 2\mathcal{R}^A(E)\mathcal{R}^B(E) \right. \\ &\quad \left. + 2\text{Re}(s_{11}^{ee}(E)s_{11}^{ee*}(-E)s_{11}^{he*}(E)s_{11}^{he}(-E)) \right] (f_{1e} - f_{2e})^2 + \frac{4e^2}{h} \int_{-\infty}^{\infty} dE \left[\mathcal{R}^A(E)\mathcal{R}^B(E) \right. \\ &\quad \left. - \text{Re}(s_{11}^{ee}(E)s_{11}^{ee*}(-E)s_{11}^{he*}(E)s_{11}^{he}(-E)) \right] (f_{1e} - f_{1h})^2. \end{aligned} \quad (16)$$

C. Δ_T noise

In this section, we provide a detailed explanation of Δ_T noise in both NQN and NQS junctions, along with the methodology

used for its computation.

This subsection discusses the Δ_T noise in an NQN junction.

1. NQN

In an NQN junction, the Δ_T noise corresponds to a shot-noise-type contribution that remains finite when the charge current vanishes in the presence of a nonzero thermovoltage. We denote this quantity as Δ_T^{NQN} , and it is calculated at the charge thermovoltage V_{th}^{NQN} , as defined in Sec. II A 1. Hence, Δ_T^{NQN} corresponds to Q_{11sh}^{NQN} in Eq. (14), evaluated at V_{th}^{NQN} . The explicit expression for Δ_T^{NQN} is:

$$\Delta_T^{NQN} = \frac{4e^2}{h} \int_{-\infty}^{\infty} dE F_{11sh}^{NQN} (f_{1e} - f_{2e})^2, \quad (17)$$

where f_{1e} and f_{2e} are evaluated at the finite thermovoltage V_{th}^{NQN} .

We also look at normalized Δ_T noise, which we define as the ratio of the Δ_T noise and conductance. For the NQN junction, normalized Δ_T noise is denoted as $\bar{\Delta}_T^{NQN}$, which is equal to $\frac{\Delta_T^{NQN}}{G_{NQN}}$, where the expression for G_{NQN} is given in Eq. (8). The normalized Δ_T noise plays a central role, as it is similar to Fano factor, which is basically the effective charge transported through the junction. Therefore, $\bar{\Delta}_T^{NQN}$ is basically a measure of the effective charge transported through the NQN junction.

2. NQS

In this subsection, we examine the behavior of Δ_T noise associated with the NQS junction. Δ_T noise in an NQS junction refers to the quantum shot noise-type contribution, evaluated at zero current and under a finite thermovoltage. It is denoted as Δ_T^{NQS} and is evaluated at the thermovoltage V_{th}^{NQS} , as defined in Sec. II A 2. Therefore, Δ_T^{NQS} corresponds to Q_{11sh}^{NQS} , given in Eq. (16), evaluated at V_{th}^{NQS} . The expression is:

$$\begin{aligned} \Delta_T^{NQS} = & \frac{4e^2}{h} \int_{-\infty}^{\infty} dE \left[\mathcal{R}^B(E)(\mathcal{T}^C(E) + \mathcal{T}^D(-E)) + \mathcal{R}^A(E) \right. \\ & (\mathcal{T}^C(-E) + \mathcal{T}^D(E)) + 2\mathcal{R}^A(E)\mathcal{R}^B(E) + 2\text{Re}(s_{11}^{ee}(E)s_{11}^{ee*}(-E) \right. \\ & \left. s_{11}^{he*}(E)s_{11}^{he}(-E)) \right] (f_{1e} - f_{2e})^2 + \frac{4e^2}{h} \int_{-\infty}^{\infty} dE \left[\mathcal{R}^A(E)\mathcal{R}^B(E) \right. \\ & \left. - \text{Re}(s_{11}^{ee}(E)s_{11}^{ee*}(-E)s_{11}^{he*}(E)s_{11}^{he}(-E)) \right] (f_{1e} - f_{1h})^2. \end{aligned} \quad (18)$$

Here, f_{1e} , f_{1h} , and f_{2e} denote the Fermi-Dirac distributions for electrons and holes in terminal 1 and for electrons in terminal 2, respectively, all evaluated at the finite charge thermovoltage V_{th}^{NQS} .

Similar to NQN junction, we also look at normalized Δ_T noise in NQS junction, which is denoted as $\bar{\Delta}_T^{NQS}$, which is

equal to $\frac{\Delta_T^{NQS}}{G_{NQS}}$, where the expression for G_{NQS} is given in Eq. (13). $\bar{\Delta}_T^{NQS}$ is a measure of the effective charge transported through the NQS junction.

III. Results and Discussion

The key results of this work are reported in this section, which is divided into two parts. First, we focus on the characteristics of (V_{th}^{NQN}) thermovoltage in NQN as well as (V_{th}^{NQS}) thermovoltage in NQS setup and further we calculate the Δ_T noise as well as quantum shot noise in NQN and NQS junctions.

A. Thermovoltage

1. NQN

In Fig. 4(a), we illustrate the behavior of the thermovoltage, denoted as V_{th}^{NQN} , as a function of the dimensionless parameter, i.e. normalized Fermi energy $\frac{E_F - V_0}{\hbar\omega_x}$, under the condition of zero net charge current. The analysis is carried out at various average temperatures: $T = 1.0K, 3.0K, \text{ and } 5.0K$, and for four distinct transport channels. For the NQN junction, V_{th}^{NQN} oscillates with increasing $\frac{E_F - V_0}{\hbar\omega_x}$. This behavior stems from the oscillating behavior of the Seebeck coefficient S_{NQN} in presence of QPC, see Fig. 4(c). Here, we ignore the range of $\frac{E_F - V_0}{\hbar\omega_x}$ between 0 to 1 as there are no QPC energy levels in that range.

2. NQS

In Fig. 4(b), we show the behavior of the thermovoltage V_{th}^{NQS} , evaluated under the same condition of zero net charge current. Below $T = 3.0K$, i.e., at $T = 0.1K$ and $1.0K$, thermal excitations are weak, and the corresponding excitation energies remain below the superconducting gap. In this low-energy regime, electron-hole (e-h) symmetry is effectively preserved because the transmission probabilities $\mathcal{R}^A(E)$ and $\mathcal{R}^B(E)$ are symmetric with respect to energy E , resulting in a vanishing charge thermovoltage, which is what is seen in Fig. 4(b). As the temperature increases, thermal excitations become stronger, enabling excitation energies to exceed the energy scale of the barrier, thereby breaking e-h symmetry and inducing a finite thermovoltage. However, as the temperature increases to $T = 3.0K, 5.0K$, thermal excitations become sufficiently strong to populate quasiparticle states above the superconducting gap, thereby breaking e-h symmetry and giving rise to a finite thermovoltage. In contrast to the oscillating trend observed in the NQN case, V_{th}^{NQS} also exhibits oscillating dependence on $\frac{E_F - V_0}{\hbar\omega_x}$. However, the magnitude of V_{th}^{NQS} at $T = 3.00K$ is small and not visible to the naked eye. However, as we increase the temperature upto $T = 5.00K$, V_{th}^{NQS} shows

prominent oscillations. This comes as a consequence of the oscillation of the Seebeck coefficient S_{NQS} as a function of $\frac{E_F - V_0}{\hbar\omega_x}$,

see Fig. 4(d).

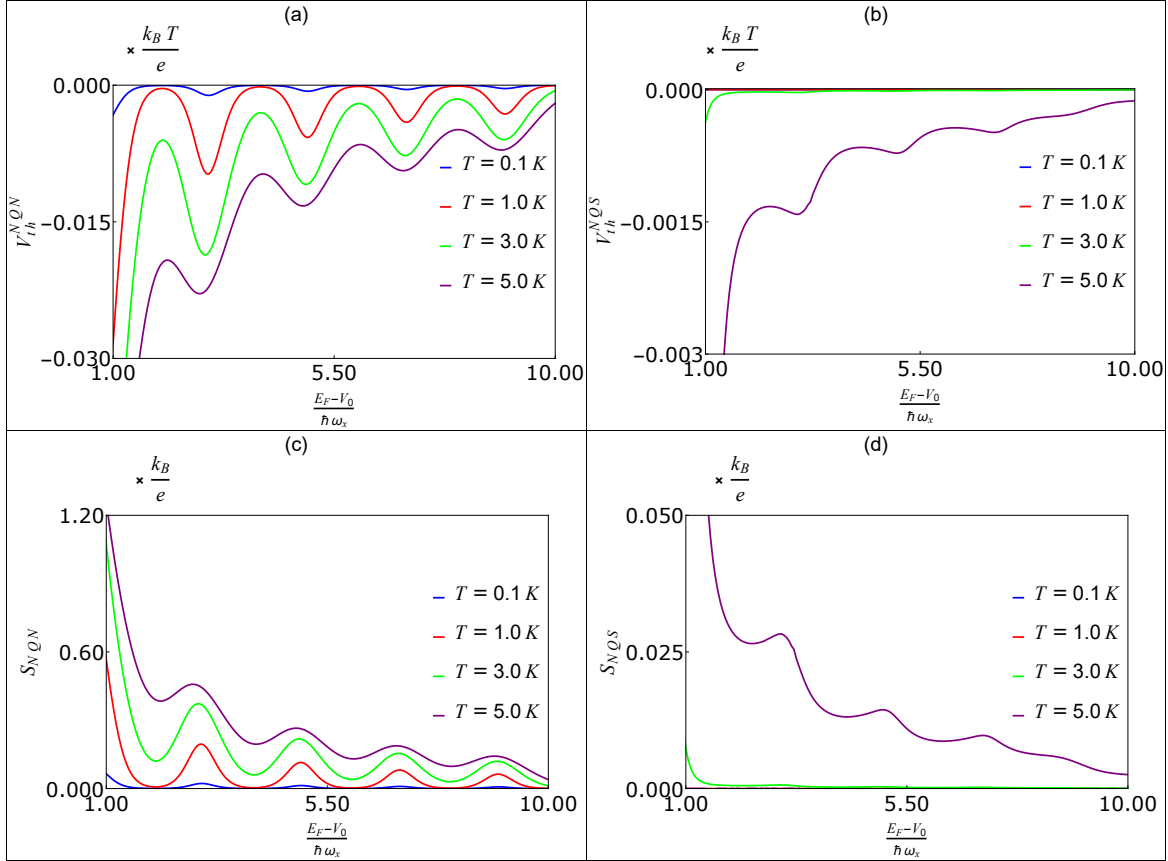


Figure 4: Charge thermovoltage in (a) NQN (V_{th}^{NQN}) and (b) NQS (V_{th}^{NQS}) (in units of $\frac{k_B T}{e}$), Seebeck coefficient in (c) NQN (S_{NQN}) and (d) NQS (S_{NQS}) (in units of $\frac{k_B}{e}$) vs. normalized Fermi energy $\frac{E_F - V_0}{\hbar\omega_x}$. The parameters taken are $n = 4$, $\hbar\omega_y = 2.73\text{meV}$, $\hbar\omega_x = 0.5\hbar\omega_y$ and $\Delta T = 0.05T$, where $T_C = 18K$.

B. Δ_T noise

1. NQN

In Fig. 5(a), we present the behavior of the charge Δ_T noise for the NQN junction, denoted by Δ_T^{NQN} , as a function of the dimensionless parameter $\frac{E_F - V_0}{\hbar\omega_x}$. The data exhibits clear oscillations in Δ_T^{NQN} as $\frac{E_F - V_0}{\hbar\omega_x}$ varies. Notably, Δ_T^{NQN} tends to approach zero in regions where the charge conductance G_{NQN} displays plateau behavior, as shown in Fig. 3(a). In contrast, peaks in Δ_T^{NQN} are observed near the transitions between conductance plateaus. This behavior is physically intuitive: in regions of perfect transmission (transparency), shot noise is suppressed, whereas across transitions, where the transmission

probability deviates from unity, the shot noise and, hence, Δ_T noise are enhanced. As the temperature increases, the amplitude of oscillations in Δ_T^{NQN} starts to reduce due to thermal broadening and the influence of finite charge thermovoltage.

2. NQS

In Fig. 5(b), we plot the corresponding Δ_T noise for the NQS junction, denoted by Δ_T^{NQS} , evaluated under the same conditions. While both NQN and NQS junctions exhibit qualitatively similar oscillatory behavior, reflecting the thermal origin of the noise. As temperature increases, the contribution from the finite thermovoltage becomes more prominent, leading to a gradual reduction in both Δ_T^{NQN} and Δ_T^{NQS} from their low-temperature values.

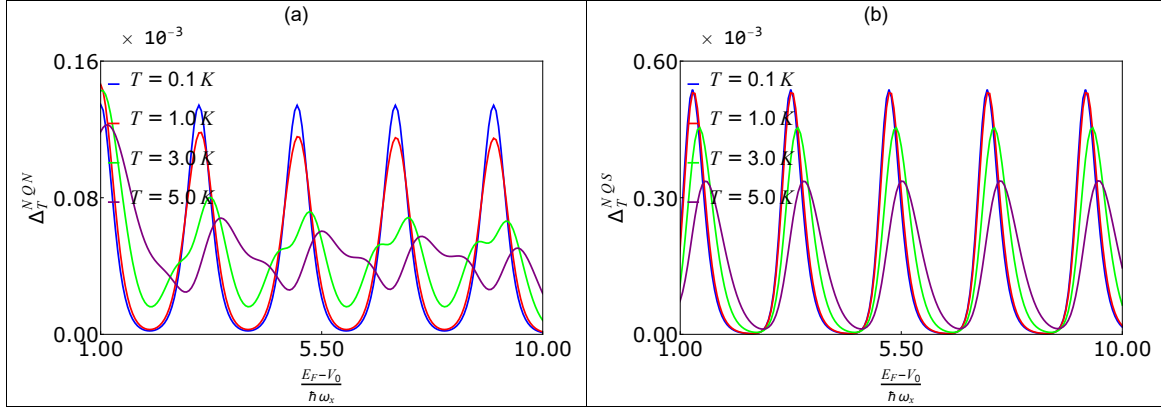


Figure 5: Charge Δ_T noise in (a) NQN (Δ_T^{NQN}) and (b) NQS (Δ_T^{NQS}) (in units of $\frac{4e^2}{h} k_B T$) vs. normalized Fermi energy $\frac{E_F - V_0}{\hbar \omega_x}$. The parameters taken are $n = 4$, $\hbar \omega_y = 2.73 \text{ meV}$, $\hbar \omega_x = 0.5 \hbar \omega_y$ and $\Delta T = 0.05 T$, where $T_C = 18 K$.

C. Quantum shot noise

1. NQN

However, when examining the quantum shot noise-like component measured at finite voltage bias, where a nonzero charge current flows, the characteristics of the noise are notably altered. As shown in Fig. 6(a), the quantum shot noise $Q_{11}^{NQN;sh}$ exhibits pronounced oscillations as a function of the dimensionless parameter $\frac{E_F - V_0}{\hbar \omega_x}$ across all temperatures considered. These oscillations reflect the energy-dependent nature of transmission in the quantum point contact and its role in noise generation. Importantly, unlike the Δ_T noise discussed earlier, the quantum shot noise lacks any secondary structures or fine features beyond the main oscillatory pattern. This distinction highlights the different physical regimes probed by Δ_T noise.

In particular, while Δ_T^{NQN} reveals thermal contributions modulated by conductance steps and thermovoltage effects, $Q_{11}^{NQN;sh}$ is primarily governed by the scattering probabilities and their energy dependence under bias.

2. NQS

When examining the quantum charge shot noise in the NQS junction at finite voltage bias, as shown in Fig. 6(b), we observe a qualitatively similar oscillatory pattern in $Q_{11}^{NQS;sh}$ as a function of $\frac{E_F - V_0}{\hbar \omega_x}$, consistent across a wide temperature range. A key observation is that the shot-noise contribution measured at finite voltage bias is significantly larger for the NQS configuration than for the NQN configuration and also do not have a unique upper bound, a contrast that does not arise when examining the corresponding Δ_T noise.

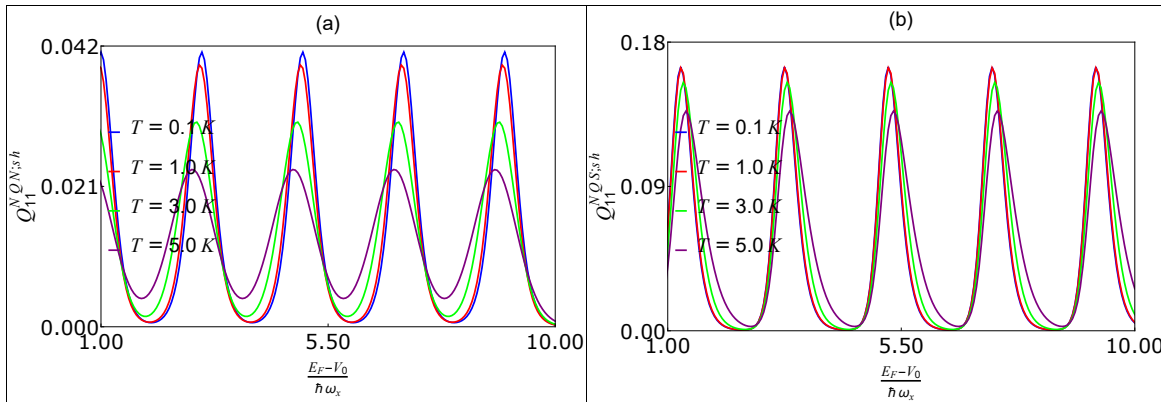


Figure 6: Charge quantum shot noise in (a) NQN ($Q_{11}^{NQN;sh}$) and (b) NQS ($Q_{11}^{NQS;sh}$) (in units of $\frac{4e^2}{h} k_B T$) vs. normalized Fermi energy $\frac{E_F - V_0}{\hbar \omega_x}$. The parameters taken are $V = \frac{k_B T}{e}$, $n = 4$, $\hbar \omega_y = 2.73 \text{ meV}$, $\hbar \omega_x = 0.5 \hbar \omega_y$ and $\Delta T = 0.05 T$, where $T_C = 18 K$.

IV. Analysis

This section analyzes our results of Δ_T noise as well as normalized Δ_T noise.

A. Δ_T noise and normalized Δ_T noise

Figure 7 illustrates a detailed examination of the Δ_T noise comparison between NQS and NQN junctions, quantified by $\frac{\Delta_T^{NQS}}{\Delta_T^{NQN}}$, as a function of the dimensionless parameter $\frac{E_F - V_0}{\hbar\omega_x}$. Our results reveal that the upper bound to the ratio is approximately around 16, see Table I, which is also seen in NIS and NIN junctions, in Ref. [13] in the transparent limit. We see the ratio approaching 16 at $T = 0.1K$, where e-h symmetry is not broken, but as the temperature increases, the ratio starts to decrease from the upper bound of 16. The primary reason for this reduction lies in the temperature regime considered in our analysis. Unlike the previous study, see Ref. [13], which focused on very low-temperature limits to emphasize pure Andreev processes and maximal electron–hole (e–h) symmetry breaking, our investigation is conducted at relatively higher temperatures. At elevated temperatures, thermal excitations become increasingly significant and tend to populate quasiparticle states above the superconducting gap. This increased excitation reduces the relative contribution of Andreev reflection to transport, thereby diminishing the amplification of noise due to e–h symmetry breaking. This leads to a reduction in the relative magnitude of charge Δ_T noise between NQS and NQN junctions, bringing it below the value of 16. This thermal suppression is consistent with earlier observations for NIS and NIN junctions, where increasing temperature was found to reduce the noise ratio in a similar manner.

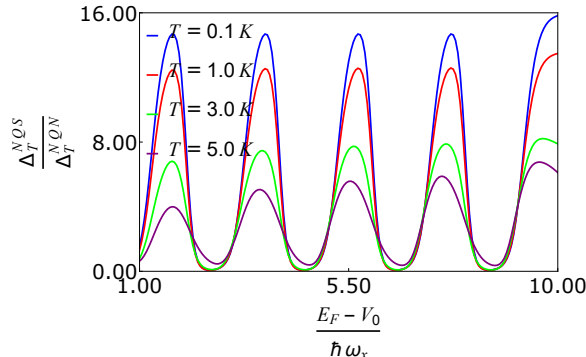


Figure 7: Ratio of Δ_T noise $\frac{\Delta_T^{NQS}}{\Delta_T^{NQN}}$ vs. $\frac{E_F - V_0}{\hbar\omega_x}$. Parameters: $n = 4$, $\hbar\omega_y = 2.73\text{meV}$, $\hbar\omega_x = 0.5\hbar\omega_y$ and $\Delta T = 0.05T$, where $T_C = 18K$.

Table I: Ratio of Δ_T noise and normalized Δ_T noise.

$\frac{\Delta_T^{NQS}}{\Delta_T^{NQN}}$	$\frac{\bar{\Delta}_T^{NQS}}{\bar{\Delta}_T^{NQN}}$
16	8

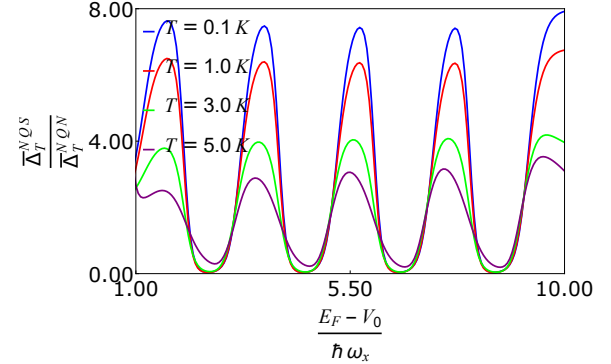


Figure 8: Ratio of normalized Δ_T noise $\frac{\Delta_T^{NQS}}{\Delta_T^{NQN}}$ vs. $\frac{E_F - V_0}{\hbar\omega_x}$. The parameters taken are $n = 4$, $\hbar\omega_y = 2.73\text{meV}$, $\hbar\omega_x = 0.5\hbar\omega_y$ and $\Delta T = 0.05T$, where $T_C = 18K$.

We proceed by examining the behavior of the normalized Δ_T noise through a comparison between NQS and NQN junctions. Focusing on the comparison between the two junction types, we find that this normalized Δ_T noise exhibits a maximum value of 8. As illustrated in Fig. 8, the normalized Δ_T noise in the NQS junction does not exceed eight times that of the NQN junction.

V. Experimental realization and Conclusion

In this work, we have investigated the impact of electron–hole (e–h) symmetry breaking on the noise characteristics of mesoscopic hybrid junctions. Specifically, we focused on Δ_T noise, in systems where a quantum point contact (QPC) serves as a tunable scatterer. By replacing the insulating barrier in conventional NIN and NIS junctions with a QPC, we deliberately break the intrinsic e–h symmetry, thereby enabling a deeper exploration of non-equilibrium transport fluctuations.

In the case of Δ_T noise, both NQN and NQS junctions exhibit clear oscillatory behavior as a function of Fermi energy. At low temperatures, we observe that the ratio $\frac{\Delta_T^{NQS}}{\Delta_T^{NQN}}$ has an upper bound of around 16. This finding are consistent to our earlier results for NIS and NIN junctions reported in Ref. [13], where a ratio of 16 was observed in the transparent limit. However, as temperature increases, the ratio reduces from 16. The primary reason for this deviation is that the present study considers a higher temperature regime where electron–hole (e–h) symmetry is broken. This symmetry breaking, combined with stronger thermal excitations, leads to a suppression of the enhancement typically attributed to Andreev processes, thereby reducing the charge Δ_T noise ratio below the value observed in low-temperature, e–h symmetric systems.

The NQN junction we study here is inspired by earlier experimental and theoretical developments in QPC-based ballistic transport [20–24]. For the superconducting segment, we consider a conventional *s*-wave superconductor with a critical temperature $T_C = 18$ K, corresponding to Nb₃Sn [33]. While our setup considers a normal metal-QPC-superconductor (NQS) geometry, similar experimental architectures, such as superconductor-QPC-superconductor junctions, have been realized [34]. These can potentially be adapted to the NQS regime by replacing one of the superconducting terminals with a normal metal.

Finally, for experimental observation of Δ_T noise, one must isolate it from the thermal noise contribution at vanishing charge current. This can be achieved by performing two measurements: one at zero temperature bias (to obtain the thermal component at zero charge current), and another at finite temperature bias (to obtain zero current quantum noise). Subtracting the former from the latter yields the Δ_T noise [10–12].

To the best of our knowledge, this is the first comprehen-

hensive theoretical study of Δ_T noise in mesoscopic normal-superconductor junctions that incorporates the effects of electron-hole symmetry breaking and studies the effect of finite charge thermovoltage. Our findings demonstrate that QPC-based hybrid structures offer a versatile and experimentally accessible platform for probing non-equilibrium fluctuation phenomena beyond the scope of conventional e-h symmetry preserving junctions.

Appendix

The Appendix is organized into four parts. In Appendix A, we present the derivation of scattering amplitudes for both NQN and NQS junctions. Appendix B then presents the evaluation of the charge current flowing through the normal-metal lead for each of these junctions considered. Subsequently, we derive charge Δ_T thermal noise auto-correlation in Appendix C.

A. Scattering amplitudes in NQN and NQS junction

The quantum point contact (QPC) was originally introduced in Ref. [27] to study conductance quantization in the ballistic transport regime. Since then, it has been widely used in the study of thermoelectric effects [21–24]. The potential landscape of the QPC is modeled by the following confinement potential [27]:

$$U(x,y) = \frac{1}{2}m^*\omega_y^2y^2 - \frac{1}{2}m^*\omega_x^2x^2 + V_0, \quad (\text{A1})$$

where m^* being electron's effective mass, and V_0 is the potential offset. The energy levels in the QPC are quantized as $E_n = V_0 + (n + 1/2)\hbar\omega_y$. The scattering amplitudes and the corresponding probabilities in a N-Q-N junction is already derived in Ref. [27] and we follow exactly the same procedure and we do not repeat the derivation here. The corresponding transmission probability for the n th mode as derived in Ref. [27] is given as

$$\mathcal{T}_Q(E) = \left(1 + e^{-2\pi(E+E_F-E_n)/\hbar\omega_x}\right)^{-1}. \quad (\text{A2})$$

We use the expression of $\mathcal{T}_Q(E)$ further for the derivation of scattering amplitudes in NQS junction. We now derive the scattering amplitudes of a N-QPC-S junction, see Fig. 9. First, we consider a N_1 -QPC- N_2 -S junction, where N_1 stands for first normal metal and N_2 stands for second normal metal, after which we calculate *s*-matrix of N-QPC-S junction. For the derivation of scattering amplitudes, we closely follow [28]. First we consider the scattering matrices of N-QPC-N junction and N-S junction separately. Thus combining both the scattering matrices for N_1 -QPC- N_2 and N_2 – S junction, we get the *s*-matrix for N-QPC-S junction in the limit, when length of the second normal metal tends to be zero. The incoming amplitudes ($c_e^+(N_1), c_e^-(N_2), c_h^-(N_1), c_h^+(N_2)$) and the outgoing amplitudes ($c_e^-(N_1), c_e^+(N_2), c_h^+(N_1), c_h^-(N_2)$) for N_1 -QPC- N_2 junction are related by a scattering matrix, which is given as

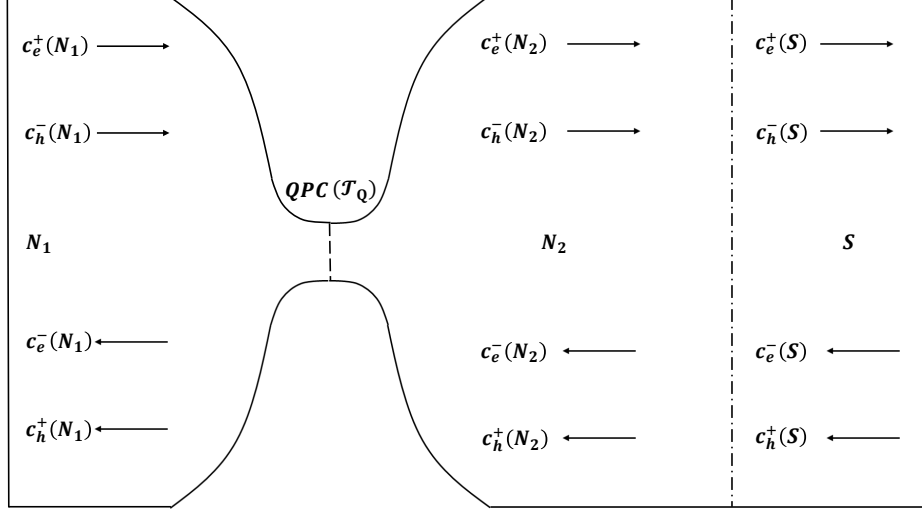


Figure 9: Schematic diagram of the $N_1 - Q - N_2 - S$ junction. The black dashed lines between $N_2 - S$ junction represent the interface between the normal metal (N) and the superconductor (S), while that in constriction between N_1 and N_2 represent the QPC with transmission probability T_Q (Eq. (A2)).

$$S_{N_1-QPC-N_2} = \begin{pmatrix} -i\sqrt{1-T_Q(E)} & \sqrt{T_Q(E)} & 0 & 0 \\ \sqrt{T_Q(E)} & -i\sqrt{1-T_Q(E)} & 0 & 0 \\ 0 & 0 & -i\sqrt{1-T_Q(-E)} & \sqrt{T_Q(-E)} \\ 0 & 0 & \sqrt{T_Q(-E)} & -i\sqrt{1-T_Q(-E)} \end{pmatrix} \quad (\text{A3})$$

Similarly, at the perfectly transparent $N_2 - S$ junction, the incoming amplitudes ($c_e^+(N_2), c_e^-(S), c_h^-(N_2), c_h^+(S)$) and the outgoing amplitudes ($c_e^-(N_2), c_e^+(S), c_h^+(N_2), c_h^-(S)$) are related by the scattering matrix, which is given as [13, 30],

$$S_{N_2-S} = \begin{pmatrix} 0 & \sqrt{|u_0|^2 - |v_0|^2}c & a & 0 \\ \sqrt{|u_0|^2 - |v_0|^2}c & 0 & 0 & -a \\ a & 0 & 0 & \sqrt{|u_0|^2 - |v_0|^2}c^* \\ 0 & -a & \sqrt{|u_0|^2 - |v_0|^2}c^* & 0 \end{pmatrix} \quad (\text{A4})$$

where $a = \frac{v_0}{u_0}$, $c = \frac{1}{u_0}$, where $u_0(v_0) = \left[\frac{1}{2} \{1 \pm \frac{\sqrt{E^2 - \Delta^2}}{E}\} \right]^{\frac{1}{2}}$ for $E > \Delta$ and for $E < \Delta$, we get $u_0(v_0) = \left[\frac{1}{2} \{1 \pm \frac{i\sqrt{\Delta^2 - E^2}}{E}\} \right]^{\frac{1}{2}}$. One can connect the incoming amplitudes ($c_e^+(N_1), c_e^-(S), c_h^-(N_1), c_h^+(S)$) and outgoing amplitudes ($c_e^-(N_1), c_e^+(S), c_h^+(N_1), c_h^-(S)$) of N_1 and S and one can get the scattering amplitudes of the N-Q-S junction. The scattering matrix of the NQS junction is given as

$$S_{NQS} = \begin{pmatrix} s_{11}^{ee}(E) & s_{12}^{ee}(E) & s_{11}^{eh}(E) & s_{12}^{eh}(E) \\ s_{21}^{ee}(E) & s_{22}^{ee}(E) & s_{21}^{eh}(E) & s_{22}^{eh}(E) \\ s_{11}^{he}(E) & s_{12}^{he}(E) & s_{11}^{hh}(E) & s_{12}^{hh}(E) \\ s_{21}^{he}(E) & s_{22}^{he}(E) & s_{21}^{hh}(E) & s_{22}^{hh}(E) \end{pmatrix}, \quad (\text{A5})$$

where $s_{lk}^{\rho\gamma}(E)$ is the amplitude for a particle of type $\gamma \in \{e, h\}$ to scatter from terminal $k \in \{1, 2\}$ to terminal $l \in \{1, 2\}$ as a particle of type $\rho \in \{e, h\}$ at energy E . The elements of the scattering matrix are given as

$$\begin{aligned}
s_{11}^{ee}(E) &= \frac{i(\sqrt{1-\mathcal{T}_Q(E)} - a^2 \sqrt{1-\mathcal{T}_Q(-E)})}{D}, & s_{12}^{ee}(E) &= -\frac{c \sqrt{\mathcal{T}_Q(E)}}{D}, & s_{11}^{eh}(E) &= -\frac{a \sqrt{\mathcal{T}_Q(E)} \sqrt{\mathcal{T}_Q(-E)}}{D}, \\
s_{12}^{eh}(E) &= -\frac{iac^* \sqrt{\mathcal{T}_Q(E)} \sqrt{1-\mathcal{T}_Q(-E)}}{D}, & s_{21}^{ee}(E) &= -\frac{c \sqrt{\mathcal{T}_Q(E)}}{D}, & s_{21}^{eh}(E) &= \frac{iac \sqrt{1-\mathcal{T}_Q(E)} \sqrt{\mathcal{T}_Q(-E)}}{D}, \\
s_{22}^{ee}(E) &= \frac{ic^2 \sqrt{1-\mathcal{T}_Q(E)}}{D}, & s_{22}^{eh}(E) &= \frac{a(1-cc^* \sqrt{1-\mathcal{T}_Q(E)} \sqrt{1-\mathcal{T}_Q(-E)}) - a^3 \sqrt{1-\mathcal{T}_Q(E)} \sqrt{1-\mathcal{T}_Q(-E)}}{D}, \\
s_{11}^{he}(E) &= -\frac{a \sqrt{\mathcal{T}_Q(E)} \sqrt{\mathcal{T}_Q(-E)}}{D}, & s_{12}^{he}(E) &= \frac{iac \sqrt{1-\mathcal{T}_Q(E)} \sqrt{\mathcal{T}_Q(-E)}}{D}, & s_{21}^{hh}(E) &= -\frac{c^* \sqrt{\mathcal{T}_Q(-E)}}{D}, \\
s_{12}^{hh}(E) &= -\frac{c^* \sqrt{\mathcal{T}_Q(-E)}}{D}, & s_{21}^{he}(E) &= -\frac{iac^* \sqrt{\mathcal{T}_Q(E)} \sqrt{1-\mathcal{T}_Q(-E)}}{D}, & s_{11}^{hh}(E) &= \frac{i(a^2 \sqrt{1-\mathcal{T}_Q(E)} - \sqrt{1-\mathcal{T}_Q(-E)})}{D}, \\
s_{22}^{hh}(E) &= -\frac{ic^{*2} \sqrt{1-\mathcal{T}_Q(-E)}}{D}, & s_{22}^{he}(E) &= -\frac{a^3 \sqrt{1-\mathcal{T}_Q(E)} \sqrt{1-\mathcal{T}_Q(-E)} + a(cc^* \sqrt{1-\mathcal{T}_Q(E)} \sqrt{1-\mathcal{T}_Q(-E)} - 1)}{D}.
\end{aligned} \tag{A6}$$

where $D = a^2 \sqrt{1-\mathcal{T}_Q(E)} \sqrt{1-\mathcal{T}_Q(-E)} - 1$. We will use these scattering matrix elements to further derive the charge current as well as general expression of charge quantum noise, which comprises of charge quantum thermal noise and charge quantum shot noise. Later, we focus on the quantum charge thermal noise at zero charge current, which is called the charge Δ_T thermal noise and quantum charge shot noise, i.e., charge Δ_T noise.

B. Average charge current in NQN and NQS junction

In mesoscopic conductors, the average current entering terminal α can be expressed within the scattering matrix framework as $\langle I_\alpha \rangle = \frac{2e}{h} \sum_\beta \int_{-\infty}^{\infty} dE (\delta_{\alpha\beta} - \mathcal{T}_{\alpha\beta}) f_\beta$. Here, $\mathcal{T}_{\alpha\beta}$ denotes the probability that an electron incident from lead β is transmitted into lead α , with the summation over β running over all connected terminals. The numerical factor of 2 accounts for spin degeneracy.

The occupation of electronic states in terminal β is described by the Fermi-Dirac function $f_\beta = \left(1 + e^{\frac{E-eV_\beta}{k_B T_\beta}}\right)^{-1}$, where V_β represents the voltage applied to terminal β and the corresponding temperature is given by $T_\beta = T + \Delta T_\beta$, with T denoting the reference equilibrium temperature and ΔT_β specifying the temperature bias at that terminal β . For the specific case of an NQN junction, involving two normal leads labeled by $\beta \in 1, 2$, the expression for the current flowing into terminal 1 simplifies to $\langle I_1 \rangle = \frac{2e}{h} \int_{-\infty}^{\infty} dE \mathcal{T}_Q(E) (f_{1e} - f_{2e})$. Here, $\mathcal{T}_Q(E)$ represents the energy-dependent transmission probability across the junction.

Similarly, in a multiterminal superconducting hybrid junction consisting of normal metal and superconductor, the charge current out of a normal metallic terminal is given as [20],

$$\langle I_\alpha \rangle = \frac{2e}{h} \sum_\beta \sum_{\rho, \xi \in \{e, h\}} \int_0^{\infty} dE \operatorname{sgn}(\rho) \left[\delta_{\alpha\beta} \delta_{\rho\xi} - \mathcal{T}_{\alpha\beta}^{\rho\xi} \right] f_\beta^{\xi}(E). \tag{B1}$$

For each terminal labeled by $\beta \in 1, 2$, the occupation probability of quasiparticle states of type $\xi \in e, h$ is described by the distribution function $f_\beta^{\xi}(E) = \left[1 + \exp\left(\frac{E + \operatorname{sgn}(\xi)V_\beta}{k_B T_\beta}\right)\right]^{-1}$, where the sign function assigns $\operatorname{sgn}(\xi) = +1$ to electron-like excitations and $\operatorname{sgn}(\xi) = -1$ to hole-like excitations, with the same convention applied to the indices ρ and η . Making use of these definitions, the expression for the charge current flowing through the normal lead of an NQS junction, as introduced in Ref. [20], can be recast into a simplified form:

$$\langle I_1 \rangle = \frac{2e}{h} \sum_\beta \sum_{\rho, \xi \in \{e, h\}} \int_0^{\infty} dE \operatorname{sgn}(\rho) \left[\delta_{1\beta} \delta_{\rho\xi} - \mathcal{T}_{1\beta}^{\rho\xi} \right] f_\beta^{\xi}(E). \tag{B2}$$

Now, the charge current in NQS junction is given as,

$$\langle I_1^{NQS} \rangle = \frac{2e}{h} \int_0^{\infty} dE (1 + \mathcal{R}_e^A(E) - \mathcal{R}_e^B(E)) (f_{1e} - f_{2e}) + \frac{2e}{h} \int_0^{\infty} dE (1 + \mathcal{R}_h^A(E) - \mathcal{R}_h^B(E)) (f_{1h} - f_{2h}) \tag{B3}$$

where $\mathcal{R}_e^A(E) = |s_{11}^{he}(E)|^2$ and $\mathcal{R}_e^B(E) = |s_{11}^{ee}(E)|^2$, $\mathcal{R}_h^A(E) = |s_{11}^{eh}(E)|^2$ and $\mathcal{R}_h^B(E) = |s_{11}^{hh}(E)|^2$. Now, utilizing the property, i.e., $s_{11}^{eh}(E) = s_{11}^{he*}(-E)$, $s_{11}^{hh}(E) = s_{11}^{ee*}(-E)$, and $f_{1h}(-E) = 1 - f_{1e}(E)$, we get the total charge current to be,

$$\langle I_1^{NQS} \rangle = \frac{2e}{h} \int_{-\infty}^{\infty} dE (1 + \mathcal{R}^A(E) - \mathcal{R}^B(E)) (f_{1e} - f_{2e}), \tag{B4}$$

where $\mathcal{R}^A(E) = \mathcal{R}_e^A(E)$, $\mathcal{R}^B(E) = \mathcal{R}_e^B(E)$.

C. Charge quantum noise and Δ_T noise in NQN and NQS junctions

The general expression of charge quantum noise Q_{ij} is given as [20, 32]

$$Q_{ij} = \frac{2e^2}{h} \int \sum_{p,q \in \{1,2\}} A_{p;l}(i, E) A_{q;k}(j, E) [f_p(E)(1 - f_q(E)) + f_q(E)(1 - f_p(E))] dE \quad (C1)$$

Here, $A_{p;l}(i, E) = \delta_{ip} \delta_{il} - s_{ip}^\dagger s_{il}$. The terms Q_{11th}^{NQN} and Q_{11sh}^{NQN} correspond to quantum thermal and quantum shot noise contributions, respectively.

Total charge quantum noise in NQN junction is $Q_{11}^{NQN} = Q_{11sh}^{NQN} + Q_{11th}^{NQN}$, where the charge shot-noise contribution (Q_{11sh}^{NQN}) and charge thermal-noise contribution (Q_{11th}^{NQN}) are given as,

$$Q_{11sh}^{NQN} = \frac{4e^2}{h} \int_{-\infty}^{\infty} dE \left[\{T_Q(1 - T_Q)\} (f_{1e} - f_{2e})^2 \right] = \frac{4e^2}{h} \int_{-\infty}^{\infty} F_{11sh}^{NQN} (f_{1e} - f_{2e})^2 dE, \quad (C2)$$

$$\text{and } Q_{11th}^{NQN} = \frac{4e^2}{h} \int_{-\infty}^{\infty} dE \left[T_Q \left(\sum_{i \in \{1,2\}} f_{ie} (1 - f_{ie}) \right) \right] = \frac{4e^2}{h} \int_{-\infty}^{\infty} F_{11th}^{NQN} \left(\sum_{i \in \{1,2\}} f_{ie} (1 - f_{ie}) \right) dE,$$

where the scattering terms depend on the QPC transmission probability T_Q , and $F_{11sh}^{NIN} = T_Q (1 - T_Q)$ while $F_{11th}^{NIN} = T_Q$.

Δ_T noise refers to the quantum shot noise-like component at finite temperature bias and vanishing current. For NQN junction, $\langle I_1^{NQN} \rangle$ is zero at finite thermovoltage V_{th}^{NQN} . Once we evaluate V_{th}^{NQN} , one can calculate Q_{11sh}^{NQN} , which is nothing but Δ_T noise, which is written as Δ_T^{NQN} for the NQN junction. Therefore, the expression for Δ_T^{NQN} is exactly same as Q_{11sh}^{NQN} as written in Eq. (C2) and is given as

$$\Delta_T^{NQN} = \frac{4e^2}{h} \int_{-\infty}^{\infty} dE \left[\{T_Q(1 - T_Q)\} (f_{1e} - f_{2e})^2 \right] = \frac{4e^2}{h} \int_{-\infty}^{\infty} F_{11sh}^{NQN} (f_{1e} - f_{2e})^2 dE \quad (C3)$$

The general expression of zero frequency charge quantum noise $Q_{ij}(\omega = \bar{\omega} = 0)$ [31], in a hybrid superconducting junction is written as,

$$Q_{ij} = \frac{2e^2}{h} \int \sum_{\substack{p,q \in \{1,2\}, \\ \mu, v, \sigma, \rho \in \{e, h\}}} sgn(\mu) sgn(v) A_{p,\sigma;q,\rho}(i\mu) A_{q,\rho;p,\sigma}(jv) (f_{p\sigma}[1 - f_{q\rho}] + (1 - f_{p\sigma}) f_{q\rho}) dE, \quad (C4)$$

where $A_{p,\sigma;q,\rho}(i\mu) = \delta_{ip} \delta_{iq} \delta_{\mu\sigma} \delta_{\mu\rho} - s_{ip}^{\mu\sigma*} s_{iq}^{\mu\rho}$. Here, for electron $sgn(\mu) = sgn(v) = +1$ and for hole, they are -1. Charge noise auto-correlation (i.e., $i = j = 1$), i.e., charge quantum noise in the normal metal of a NQS junction, is,

$$Q_{11}^{NQS} = \frac{2e^2}{h} \int \sum_{\substack{p,q \in \{1,2\}, \\ \mu, v, \sigma, \rho \in \{e, h\}}} sgn(\mu) sgn(v) A_{p,\sigma;q,\rho}(1\mu) A_{q,\rho;p,\sigma}(1v) (f_{p\sigma}[1 - f_{q\rho}] + (1 - f_{p\sigma}) f_{q\rho}) dE, \quad (C5)$$

Using the s -matrix as shown in Eq. (B3), charge quantum noise auto-correlation can be simplified as,

$$Q_{11}^{NQS} = Q_{11th}^{NQS} + Q_{11sh}^{NQS}, \quad (C6)$$

where,

$$Q_{11th}^{NQS} = \frac{4e^2}{h} \int_{-\infty}^{\infty} dE \left[(1 - \mathcal{R}^B(E) + \mathcal{R}^A(E))^2 + \mathcal{R}^A(-E) \mathcal{R}^B(E) + \mathcal{R}^A(E) \mathcal{R}^B(-E) + \mathcal{R}^B(E) (\mathcal{T}^C(E) + \mathcal{T}^D(-E)) \right. \\ \left. + \mathcal{R}^A(E) (\mathcal{T}^D(E) + \mathcal{T}^C(-E) + 2\mathcal{R}^A(E) \mathcal{R}^B(E)) \right] f_{1e} (1 - f_{1e}) + \frac{4e^2}{h} \int_{-\infty}^{\infty} dE \left[\mathcal{T}^C(E)^2 + \mathcal{T}^D(E)^2 \right. \\ \left. + 2\mathcal{T}^C(E) \mathcal{T}^D(-E) + \mathcal{R}^B(E) (\mathcal{T}^C(E) + \mathcal{T}^D(-E)) + \mathcal{R}^A(E) (\mathcal{T}^C(-E) + \mathcal{T}^D(E)) \right] f_{2e} (1 - f_{2e}), \quad (C7)$$

$$Q_{11sh}^{NQS} = \frac{4e^2}{h} \int_{-\infty}^{\infty} dE \left[\mathcal{R}^B(E) (\mathcal{T}^C(E) + \mathcal{T}^D(-E)) + \mathcal{R}^A(E) (\mathcal{T}^C(-E) + \mathcal{T}^D(E)) + 2\mathcal{R}^A(E) \mathcal{R}^B(E) \right. \\ \left. + 2Re(s_{11}^{ee}(E) s_{11}^{ee*}(-E) s_{11}^{he*}(E) s_{11}^{he}(-E)) \right] (f_{1e} - f_{2e})^2 + \frac{4e^2}{h} \int_{-\infty}^{\infty} dE \left[\mathcal{R}^A(E) \mathcal{R}^B(E) \right. \\ \left. - Re(s_{11}^{ee}(E) s_{11}^{ee*}(-E) s_{11}^{he*}(E) s_{11}^{he}(-E)) \right] (f_{1e} - f_{1h})^2.$$

Here, Q_{11th}^{NQS} and Q_{11sh}^{NQN} are the thermal and shot noise-like component in NQS junction. The various scattering mechanisms are described in terms of their associated probabilities, where Andreev reflection is represented by $\mathcal{R}^A(E) = |s_{11}^{he}(E)|^2$ and the normal reflection probability is given by $\mathcal{R}^B(E) = |s_{11}^{ee}(E)|^2$. In addition, the transmission of quasiparticles across the junction is quantified by $\mathcal{T}^C(E) = |s_{21}^{ee}(E)|^2$ for electron-like excitations and by $\mathcal{T}^D(E) = |s_{21}^{he}(E)|^2$ for hole-like excitations, both evaluated at energy E . Similarly, one can also calculate the scattering probabilities such as $\mathcal{R}^A(-E)$, $\mathcal{R}^B(-E)$, $\mathcal{T}^C(-E)$ and $\mathcal{T}^D(-E)$ by replacing E by $-E$ in the expressions of scattering probabilities.

Here, Δ_T noise for NQN junction is same as Q_{11sh}^{NQS} at non-zero temperature bias and vanishing current. In the NQS junction, the charge current $\langle I_1^{NQS} \rangle = 0$ is achieved at thermovoltage V_{th}^{NQS} . Then, Q_{11sh}^{NQS} can be evaluated at finite V_{th}^{NQS} , which is equal to Δ_T^{NQS} . Therefore, the expression for Δ_T^{NQS} is exactly same as Q_{11sh}^{NQS} as written in Eq. (C7) and is given as

$$\begin{aligned} \Delta_T^{NQS} = & \frac{4e^2}{h} \int_{-\infty}^{\infty} dE \left[\mathcal{R}^B(E)(\mathcal{T}^C(E) + \mathcal{T}^D(-E)) + \mathcal{R}^A(E)(\mathcal{T}^C(-E) + \mathcal{T}^D(E)) + 2\mathcal{R}^A(E)\mathcal{R}^B(E) \right. \\ & + 2\text{Re}(s_{11}^{ee}(E)s_{11}^{ee*}(-E)s_{11}^{he*}(E)s_{11}^{he}(-E)) (f_{1e} - f_{2e})^2 + \frac{4e^2}{h} \int_{-\infty}^{\infty} dE \left[\mathcal{R}^A(E)\mathcal{R}^B(E) \right. \\ & \left. \left. - \text{Re}(s_{11}^{ee}(E)s_{11}^{ee*}(-E)s_{11}^{he*}(E)s_{11}^{he}(-E)) \right] (f_{1e} - f_{1h})^2. \right] \end{aligned} \quad (\text{C8})$$

[1] J. Eriksson, M. Acciai, L. Tesser, and J. Splettstoesser, General bounds on electronic shot noise in the absence of currents, *Phys. Rev. Lett.* **127**, 136801 (2021).

[2] J. Rech, T. Jonckheere, B. Grémaud, and T. Martin, Negative delta- t noise in the fractional quantum hall effect, *Phys. Rev. Lett.* **125**, 086801 (2020).

[3] G. Zhang, I. V. Gornyi, and C. Spaanslatt, Delta- t noise for weak tunneling in one-dimensional systems: Interactions versus quantum statistics, *Phys. Rev. B* **105**, 195423 (2022).

[4] L. Tesser, M. Acciai, C. Spaanslatt, J. Monsel, and J. Splettstoesser, Charge, spin, and heat shot noises in the absence of average currents: Conditions on bounds at zero and finite frequencies, *Phys. Rev. B* **107**, 075409 (2023).

[5] M. Hein and C. Spaanslatt, Thermal conductance and noise of majorana modes along interfaced $\nu = \frac{5}{2}$ fractional quantum hall states, *Phys. Rev. B* **107**, 245301 (2023).

[6] S. Larocque, E. Pinsolle, C. Lupien, and B. Reulet, Shot noise of a temperature-biased tunnel junction, *Phys. Rev. Lett.* **125**, 106801 (2020).

[7] M. Hübner and W. Belzig, Light emission in delta- T -driven mesoscopic conductors, *Phys. Rev. B* **107**, 155405 (2023).

[8] R. A. Melcer, B. Dutta, C. Spaanslatt, J. Park, A. D. Mirlin, and V. Umansky, Absent thermal equilibration on fractional quantum hall edges over macroscopic scale, *Nature communications* **13**, 376 (2022).

[9] A. Popoff, J. Rech, T. Jonckheere, L. Raymond, B. Grémaud, S. Malherbe, and T. Martin, Scattering theory of non-equilibrium noise and delta t current fluctuations through a quantum dot, *Journal of Physics: Condensed Matter* **34**, 185301 (2022).

[10] O. S. Lumbroso, L. Simine, A. Nitzan, D. Segal, and O. Tal, Electronic noise due to temperature differences in atomic-scale junctions, *Nature* **562**, 240 (2018).

[11] O. Shein-Lumbroso, Electronic noise in atomic and molecular junctions: Beyond the known noise contributions, *PhD Thesis* Weizmann Institute of Science (2022).

[12] E. Sivre, H. Duprez, A. Anthore, A. Aassime, F. Parmentier, A. Cavanna, A. Ouerghi, U. Gennser, and F. Pierre, Electronic heat flow and thermal shot noise in quantum circuits, *Nature Communications* **10**, 5638 (2019).

[13] S. Mishra, A. R. Dora, T. Mohapatra, and C. Benjamin, Δ_T noise in mesoscopic hybrid junctions: influence of barrier strength and thermal bias, *Journal of Physics: Condensed Matter* **37**, 465302 (2025).

[14] L. Pierattelli, F. Taddei, and A. Braggio, Δ_T -noise in multiterminal hybrid systems, *Phys. Rev. Res.* **7**, 023321 (2025).

[15] S. Mishra and C. Benjamin, Probing the dichotomy between Yu-Shiba-Rusinov and Majorana bound states via conductance, quantum noise, and Δ_T noise, *Phys. Rev. B* **112**, 024505 (2025).

[16] S. Mishra and C. Benjamin, Negative spin Δ_T noise induced by spin-flip scattering and andreev reflection (2025), [arXiv:2307.14072 \[cond-mat.mes-hall\]](https://arxiv.org/abs/2307.14072).

[17] O. Shein-Lumbroso, M. Gerry, A. Shastry, A. Vilan, D. Segal, and O. Tal, Delta-T flicker noise demonstrated with molecular junctions, *Nano Letters* **24**, 1981 (2024).

[18] K. Iyer, J. Rech, T. Jonckheere, L. Raymond, B. Grémaud, and T. Martin, Colored delta- T noise in fractional quantum hall liquids, *Phys. Rev. B* **108**, 245427 (2023).

[19] The Mathematica codes are available: <https://github.com/Sachiraj/QPC-Delta-T.git>.

[20] G. Benenti, G. Casati, K. Saito, and R. Whitney, Fundamental aspects of steady-state conversion of heat to work at the nanoscale, *Physics Reports* **694**, 1 (2017).

[21] B. J. van Wees, H. van Houten, C. W. J. Beenakker, J. G. Williamson, L. P. Kouwenhoven, D. van der Marel, and C. T. Foxon, Quantized conductance of point contacts in a two-dimensional electron gas, *Phys. Rev. Lett.* **60**, 848 (1988).

[22] D. Wharam, T. J. Thornton, R. Newbury, M. Pepper, H. Ahmed, J. Frost, D. Hasko, D. Peacock, D. Ritchie, and G. Jones, One-dimensional transport and the quantisation of the ballistic resistance, *Journal of Physics C: solid state physics* **21**, L209 (1988).

[23] H. Van Houten, L. Molenkamp, C. Beenakker, and C. Foxon, Thermo-electric properties of quantum point contacts, *Semiconductor Science and Technology* **7**, B215 (1992).

[24] L. W. Molenkamp, T. Gravier, H. van Houten, O. J. A. Buijk, M. A. A. Mabesoone, and C. T. Foxon, Peltier coefficient and thermal conductance of a quantum point contact, *Phys. Rev. Lett.* **68**, 3765 (1992).

[25] Y. M. Blanter and M. Büttiker, Shot noise in mesoscopic con-

ductors, Physics reports **336**, 1 (2000).

[26] S. Datta, [Electronic Transport in Mesoscopic Systems](#), Cambridge Studies in Semiconductor Physics and Microelectronic Engineering (Cambridge University Press, 1995).

[27] M. Büttiker, Quantized transmission of a saddle-point constriction, [Phys. Rev. B](#) **41**, 7906 (1990).

[28] C. W. J. Beenakker, Quantum transport in semiconductor-superconductor microjunctions, [Phys. Rev. B](#) **46**, 12841 (1992).

[29] C. W. J. Beenakker, Random-matrix theory of quantum transport, [Rev. Mod. Phys.](#) **69**, 731 (1997).

[30] G. E. Blonder, M. Tinkham, and T. M. Klapwijk, Transition from metallic to tunneling regimes in superconducting microconstrictions: Excess current, charge imbalance, and supercurrent conversion, [Phys. Rev. B](#) **25**, 4515 (1982).

[31] M. P. Anantram and S. Datta, Current fluctuations in mesoscopic systems with andreev scattering, [Phys. Rev. B](#) **53**, 16390 (1996).

[32] T. Martin, Course 5 noise in mesoscopic physics, in [Les Houches](#), Vol. 81 (Elsevier, 2005) pp. 283–359.

[33] B. T. Matthias, T. H. Geballe, S. Geller, and E. Corenzwit, Superconductivity of nb_3sn , [Phys. Rev.](#) **95**, 1435 (1954).

[34] L. Bretheau, Ç. Girit, H. Pothier, D. Esteve, and C. Urbina, Exciting andreev pairs in a superconducting atomic contact, [Nature](#) **499**, 312 (2013).